INTERNATIONAL JOURNAL FOR NUMERICAL AND ANALYTICAL METHODS IN GEOMECHANICS, VOL. 21, 361–378 (1997)

SURFACE DISPLACEMENTS OF A NON-HOMOGENEOUS ELASTIC HALF-SPACE SUBJECTED TO UNIFORM SURFACE TRACTIONS. PART I: LOADING ON ARBITRARILY SHAPED AREAS

R. F. STARK* AND J. R. BOOKER

School of Civil and Mining Engineering, University of Sydney, N.S.W. 2006, Australia

SUMMARY

A numerical technique is presented for the analysis of surface displacements of a non-homogeneous elastic half-space subjected to vertical and/or horizontal surface loads uniformly distributed over an arbitrarily shaped area. The non-homogeneity considered is a particular form of power variation of Young's modulus with depth. Since the exponent which determines the degree of non-homogeneity may vary from zero to unity, both the homogeneous half-space and the Gibson soil may be included as limiting cases in a single numerical scheme. In order to account for the arbitrary shape of the loading, the boundary of the loaded area is linearized piecemeal. This enables the modeling of any load pattern according to the desired degree of accuracy. Special attention is focused on the integration scheme, since the singularity associated with the Green's function becomes progressively more pronounced the greater the non-homogeneity parameter gets. The performance of the numerical procedure is studied using analytical solutions for rectangular shaped areas. Further comparisons with well-known solutions based on integral transform techniques for a uniformly distributed load acting on a circular area of the non-homogeneous soil mass show excellent agreement as well.

Int. J. Numer. Anal. Meth. Geomech., Vol. 21, 361–378 (1997)
(No. of Figures: 13 No. of Tables: 1 No. of Refs: 19)

Key words: elastic half-space; homogeneous; non-homogeneous; contour integral approach; surface displacement; arbitrarily shaped loading area

1. INTRODUCTION

In geotechnical engineering there is a class of problem where the application of the theory of elasticity seems reasonable, despite the fact that real soil behaviour is far from being adequately described as linearly elastic. For the analysis of raft foundations for instance, it is usually justified to assume linear elastic soil response within the range of working loads, since those regions where

* Correspondence to: R. F. Stark, Institute for Strength of Materials, University of Innsbruck, Technikerstr. 13, A-6020 Innsbruck, Austria

Contract grant sponsor: Austrian Science Foundation; contract grant number: J0702-Tec; contract grant number: J0963-Tec

CCC 0363–9061/97/060361–18$17.50

Received 17 March 1995
Revised 27 August 1996

yielding will occur usually remain small compared with the overall area of the soil–structure interface.

Certainly, results from the theory of elasticity based on the assumption of homogeneity may be reasonable for a first estimate. However, in natural soil deposits the stiffness usually increases with depth due to the increasing overburden pressure, hence being in contradiction to the assumption of homogeneity. This fact has been recognized, and some attempt has been made to analyse the behaviour of footings resting on a soil mass whose modulus increases linearly with depth. Gibson[1] and Brown and Gibson[2], for instance, have studied the half-space exhibiting this kind of non-homogeneity, whereas Gibson *et al.*[3] have considered the behaviour of a finite layer whose modulus increases linearly with depth. Fischer[4] proposed to linearize the variation of Young's modulus for each layer. Rowe and Booker[5,6] studied the behaviour of footings on a non-homogeneous layered soil mass by using a finite layer approach. Other methods which account for the fact of non-homogeneity by assuming some kind of linear variation of Young's modulus have been suggested by Repnikov,[7] Schultze,[8] Giroud,[9] and Butler.[10] Models based on the assumption of linearly increasing Young's modulus E may be particularly useful for deep clay deposits but there is some evidence that for sands E is more likely to vary non-linearly with depth z below the surface. Fröhlich,[11] Ohde,[12] and Holl[13] investigated specific combinations between the variation of Young's modulus with depth and different invariable Poisson's ratio v. Booker *et al.*[14,15] have studied this case in a more general form and published solutions for the stress and displacement fields due to line loads and point loads and their application to simple loading patterns, such as strips and circles.

In current engineering practice the finite element method is well established and has proved to be a useful tool for the analysis of raft foundations. Usually, the foundation structure is discretized by finite elements whereas the mechanical behaviour of the soil base is modelled by appropriate analytical or numerical solutions. The technique, probably most widely used, applies the Winkler approach despite its obvious physical shortcomings. The reasons for that is firstly that most of the available finite element programs provide the option of Winkler-type foundation and secondly that there is no restriction with respect to the shape of finite elements to be used. On the other hand, the continuum model approach based on the theory of elasticity is commonly accepted as a method whose results tend to be in much closer agreement with the reality. However, this technique usually employs analytical solutions for the surface displacements and therefore methods like those proposed by Cheung and Zienkiewicz[16] or Chow,[17] impose the restriction of using only rectangular or square shaped elements.

Based on the results published by Booker *et al.*[14,15] this paper describes a numerical procedure to determine the surface displacements of a non-homogeneous soil mass subjected to uniformly distributed surface tractions. Using this approach, both homogeneous and non-homogeneous soil bases may be analysed within the same framework. The loaded area may have any arbitrary shape. In the numerical procedure the boundary of the loaded region is linearly approximated. Since there is no limitation with respect to the order of polygon, any shape of loaded area may be handled to the desired degree of accuracy. As an example, this process will be demonstrated to trace the approximation of a circular area with different regular polygons in order to check the proposed numerical scheme.

With respect to finite element applications, the method proposed allows the computation of the flexibility coefficients, say, on the basis of the actual shape of the element under consideration, rather than working with a 'substitute rectangular or circular element' of equivalent area. It will be shown that by appropriate transformation the singularity associated with the Green's function does not constitute any problem, since the solution is found by integrating solely over the boundary of the loaded area.

2. SURFACE DISPLACEMENTS OF THE NON-HOMOGENEOUS HALF-SPACE

In the following derivation it is assumed that the soil mass can be idealized as an isotropic but non-homogeneous medium whose elastic constants are given by

$$\begin{aligned} E(z) &= m_E z^{\alpha}, \quad 0 \leqslant \alpha \leqslant 1 \\ \nu(z) &= \nu = \text{const.} \end{aligned} \tag{1}$$

where m_E is a constant which determines Young's modulus at the depth $z = 1$, α is referred to as the non-homogeneity parameter and ν denotes Poisson's ratio. Figure 1 shows schematically the variation of Young's modulus with the depth for some values of α. It might be interesting to notice that for the homogeneous half-space ($\alpha = 0$), m_E has the dimension of Young's modulus, whereas for the Gibson soil ($\alpha = 1$), m_E takes the dimension of the modulus of subgrade reaction.

The starting point for the calculation of the surface displacements of the non-homogeneous half-space caused by a surface traction distributed on an arbitrarily shaped area is the fundamental solution for the point load given by Booker *et al.*[14] The displacement vector of any point $(x, y, 0)$ of the surface of the half-space due to a point load acting at the location $(\xi, \eta, 0)$ is given by the following matrix equation:

$$\mathbf{u}_P = \mathbf{G}\mathbf{P} \tag{2}$$

where

$$\mathbf{G} = \frac{1}{m_E R^{(\alpha+3)}} \begin{bmatrix} H(x-\xi)^2 + K(y-\eta)^2 & (H-K)(x-\xi)(y-\eta) & A(x-\xi)R \\ (H-K)(x-\xi)(y-\eta) & H(y-\eta)^2 + K(x-\xi)^2 & A(y-\eta)R \\ L(x-\xi)R & L(y-\eta)R & BR^2 \end{bmatrix} \tag{3}$$

and

$$\begin{aligned} \mathbf{u}_P &= (u_x, u_y, u_z)^T \\ \mathbf{P} &= (P_x, P_y, P_z)^T \end{aligned} \tag{4}$$

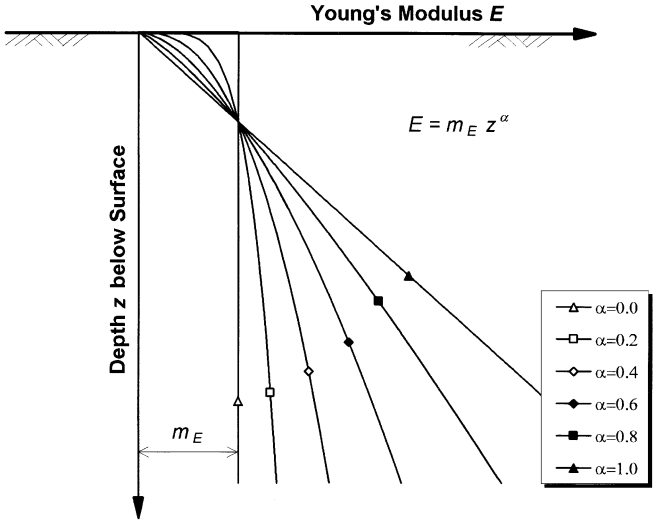

Figure 1. Variation of Young's modulus with depth for different degrees of non-homogeneity

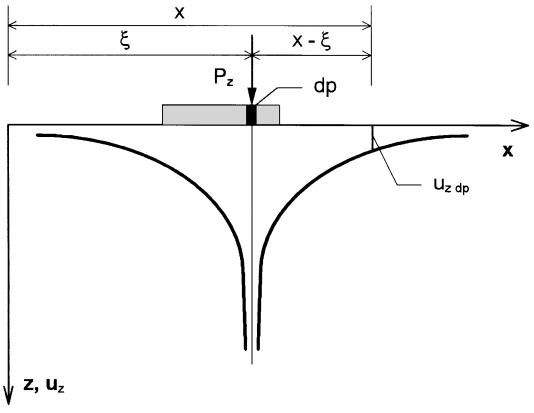

Figure 2. Axisymmetric deflection profile in section $y = 0$ due to 'point load' dp

R is the distance between the location where the surface displacement is sought and the point where the load is applied, i.e.

$$R = \sqrt{(x - \xi)^2 + (y - \eta)^2} = \sqrt{u^2 + v^2} \tag{5}$$

and the parameters A, B, H, K, L are defined in the appendix.

On integrating the fundamental solution of the non-homogeneous half-space given by (2) several solutions of practical interest may be obtained. Booker *et al.*[15] gave closed-form solutions for the uniformly loaded strip and the uniformly loaded ring and circular area, as well as for the smooth rigid strip and the smooth rigid circular footing.

To calculate the surface displacement due to a distributed load $\mathbf{p}(\xi, \eta)$ acting over an arbitrarily shaped region, Ω, of the surface of a non-homogeneous half-space, for the sake of simplicity we start with the axisymmetric problem of a point load acting perpendicular to the surface of the half-space, as shown in Figure 2.

For the time being, we will focus attention only on the vertical displacement caused by the vertical component of the point load, i.e. $\mathbf{P} = (0, 0, P_z)^{\mathrm{T}}$. The axisymmetric solution for this case is then given by

$$u_{zz}(x, y) = \frac{BP_z}{m_E R^{(\alpha+1)}} \tag{6}$$

Setting $P_z = p_z(\xi, \eta)\,\mathrm{d}\xi\,\mathrm{d}\eta$ and integrating over the loaded area, Ω, the displacement, $u_{zz}(x, y)$, is found to be

$$u_{zz}(x, y) = \frac{B}{m_E} \int\int_{\Omega} \frac{p_z(\xi, \eta)}{R^{(\alpha+1)}}\,\mathrm{d}\xi\,\mathrm{d}\eta \tag{7}$$

If p_z is set to constant unit pressure, u_{zz} then would represent the flexibility coefficient f_{zz}. Rewriting equation (7) in a more general form we get

$$u_{rs} = p_s \int\int_{\Omega} G_{rs}\,\mathrm{d}\xi\,\mathrm{d}\eta \tag{8}$$

where u_{rs} is the displacement in direction r due to the uniformly distributed loading p_s acting on Ω parallel to s and G_{rs} is a particular element of the matrix $\mathbf{G}$ given by equation (3).

3. INTEGRATION ALGORITHM

In this section an integration algorithm for equation (8) is developed. For the kind of shape commonly used in finite element techniques like quadrilaterals and triangles, (8) is usually integrated by applying a Gauss–Legendre quadrature scheme. However, numerical problems might arise when the distance between field point and load point tends to zero, a situation which is very likely to occur when, say, the flexibility coefficient f_{ij}, $i = j$ is evaluated. Depending on the degree of non-homogeneity, the integral in (8) varies between type 'weak singular' in the case of the homogeneous half-space, i.e. $\alpha = 0$, and type 'strong singular' in the case of the Gibson soil, i.e. $\alpha = 1$. Whereas for the homogeneous case Gauss–Legendre quadrature scheme will lead to acceptable results in most cases, the error involved becomes more pronounced the stronger the singularity gets. The other aim is to provide a numerical integration procedure which may be used to deal with any shape of the loaded region.

The basic idea is to make use of the Gaussian theorem by which an integration over a three-dimensional domain can be replaced with the integration over its boundary surface alone, i.e.

$$\int_{\Omega} \nabla \cdot \mathbf{v} \, d\Omega = \int_{\Gamma} \mathbf{v} \cdot \mathbf{n} \, d\Gamma . \tag{9}$$

In (9) $\mathbf{v}$ is a vector function, Ω is the integration domain confined by its surface boundary Γ and $\mathbf{n}$ is the outward directed normal vector on Γ. The Hamilton operator ∇ is defined by

$$\nabla = \left(\frac{\partial}{\partial x}, \frac{\partial}{\partial y}, \frac{\partial}{\partial z} \right)^{\mathrm{T}} \tag{10}$$

If

$$\mathbf{v} = \nabla \phi = \operatorname{grad} \phi \tag{11}$$

where ϕ is a scalar function, then (9) becomes

$$\int_{\Omega} \nabla^2 \phi \, d\Omega = \int_{\Gamma} \nabla \phi \cdot \mathbf{n} \, d\Gamma = \int_{\Gamma} \frac{\partial \phi}{\partial n} \, d\Gamma \tag{12}$$

Interpreting equation (12) for our problem Ω represents the loaded area of the half-space and Γ denotes its boundary, as shown in Figure 3.

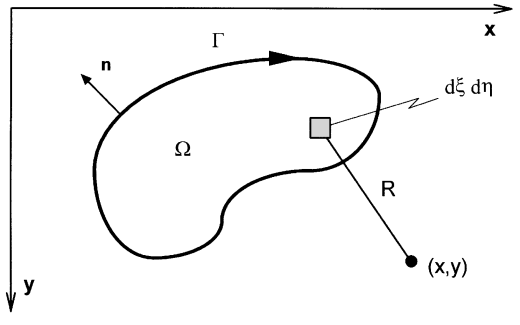

Figrue 3. Integration domain

The integral on the right-hand side of (12) has to be taken in a clockwise direction around the complete closed boundary if a right twisting co-ordinate system is used, as shown in Figure 3 where the xy-plane is attached to the surface of the half-space. This implies that a vertical pressure loading on the surface of the half-space is taken positively and will result in positive vertical displacements, which is consistent with the usual convention in soil mechanics, taking compressive stresses and strains as positive quantities.

Let

$$\nabla^2 \mathbf{\Phi} = m_E \mathbf{G} = \mathbf{\Psi} \tag{13}$$

where $\mathbf{G}$, given by (3), is expressed by $\mathbf{\Psi}$ taking the form

$$\mathbf{\Psi} = \begin{bmatrix} \dfrac{(H+K)}{2}\psi_4 + \dfrac{(H-K)}{2}\psi_5 & (H-K)\psi_6 & A\psi_2 \\ (H-K)\psi_6 & \dfrac{(H+K)}{2}\psi_4 - \dfrac{(H-K)}{2}\psi_5 & A\psi_3 \\ L\psi_2 & L\psi_3 & B\psi_1 \end{bmatrix} \tag{14}$$

The coefficients A, B, H, K and L are given in the appendix and the functions ψ_i, $i = 1, 2, \ldots, 6$ are defined by

$$\begin{aligned} \psi_1 &= R^{\gamma_1} \\ \psi_2 &= uR^{\gamma_2} \\ \psi_3 &= vR^{\gamma_3} \\ \psi_4 &= (u^2 + v^2)R^{\gamma_4} \\ \psi_5 &= (u^2 - v^2)R^{\gamma_5} \\ \psi_6 &= uvR^{\gamma_6} \end{aligned} \tag{15}$$

where R, u and v are defined by (5) and γ_i, $i = 1, 2, \ldots, 6$ are given by

$$\begin{aligned} \gamma_1 &= -(\alpha + 1) \\ \gamma_2 &= -(\alpha + 2) = \gamma_3 \\ \gamma_4 &= -(\alpha + 3) = \gamma_5 = \gamma_6 \end{aligned} \tag{16}$$

It can be shown (Stark and Booker[18]) that the matrix $\mathbf{\Phi}$ defined as follows

$$\mathbf{\Phi} = \begin{bmatrix} \dfrac{(H+K)}{2}\phi_4 + \dfrac{(H-K)}{2}\phi_5 & (H-K)\phi_6 & A\phi_2 \\ (H-K)\phi_6 & \dfrac{(H+K)}{2}\phi_4 - \dfrac{(H-K)}{2}\phi_5 & A\phi_3 \\ L\phi_2 & L\phi_3 & B\phi_1 \end{bmatrix} \tag{17}$$

will satisfy equation (13) if the individual functions ϕ_i, $i = 1, 2, \ldots, 6$ take the form given below

$$\begin{aligned}
\phi_1 &= \frac{R^{(\gamma_1+2)}}{(\gamma_1+2)^2} \\
\phi_2 &= \frac{uR^{(\gamma_2+2)}}{(\gamma_2+2)(\gamma_2+4)} \\
\phi_3 &= \frac{vR^{(\gamma_3+2)}}{(\gamma_3+2)(\gamma_3+4)} \\
\phi_4 &= \frac{R^{(\gamma_4+4)}}{(\gamma_4+4)^2} \\
\phi_5 &= \frac{(u-v)^2 R^{(\gamma_5+2)}}{(\gamma_5+2)(\gamma_5+6)} \\
\phi_6 &= \frac{uvR^{(\gamma_6+2)}}{(\gamma_6+2)(\gamma_6+6)}
\end{aligned} \tag{18}$$

Rewriting the integrand of the right-hand side of (12) for our case we get

$$\frac{\partial \mathbf{\Phi}}{\partial n} = \frac{\partial \mathbf{\Phi}}{\partial \xi} n_\xi + \frac{\partial \mathbf{\Phi}}{\partial \eta} n_\eta \tag{19}$$

Evaluating the derivatives of the individual functions ϕ_i with respect to n, making use of (16) and noticing that $L = -A$, some rearrangement finally yields the elements of the matrix $\partial\mathbf{\Phi}/\partial n$.

$$\begin{aligned}
\frac{\partial \Phi_{xx}}{\partial n} &= \frac{(H+K)}{2(\alpha-1)} \frac{(un_\xi + vn_\eta)}{R^{(\alpha+1)}} + \frac{(H-K)}{2(3-\alpha)R^{(\alpha+1)}} \left[\frac{2(un_\xi - vn_\eta)}{(\alpha+1)} - \frac{(u^2-v^2)(un_\xi+vn_\eta)}{R^2} \right] \\
\frac{\partial \Phi_{xy}}{\partial n} &= \frac{(H-K)}{(3-\alpha)R^{(\alpha+1)}} \left[\frac{(un_\eta + vn_\xi)}{(\alpha+1)} - \frac{uv(un_\xi+vn_\eta)}{R^2} \right] = \frac{\partial \Phi_{yx}}{\partial n} \\
\frac{\partial \Phi_{xz}}{\partial n} &= \frac{A}{(2-\alpha)R^\alpha} \left[\frac{n_\xi}{\alpha} - \frac{u(un_\xi+vn_\eta)}{R^2} \right] = -\frac{\partial \Phi_{zx}}{\partial n} \\
\frac{\partial \Phi_{yy}}{\partial n} &= \frac{(H+K)}{2(\alpha-1)} \frac{(un_\xi + vn_\eta)}{R^{(\alpha+1)}} - \frac{(H-K)}{2(3-\alpha)R^{(\alpha+1)}} \left[\frac{2(un_\xi - vn_\eta)}{(\alpha+1)} - \frac{(u^2-v^2)(un_\xi+vn_\eta)}{R^2} \right] \\
\frac{\partial \Phi_{yz}}{\partial n} &= \frac{A}{(2-\alpha)R^\alpha} \left[\frac{n_\eta}{\alpha} - \frac{v(un_\xi+vn_\eta)}{R^2} \right] = -\frac{\partial \Phi_{zy}}{\partial n} \\
\frac{\partial \Phi_{zz}}{\partial n} &= \frac{B}{(\alpha-1)} \frac{(un_\xi+vn_\eta)}{R^{(\alpha+1)}}
\end{aligned} \tag{20}$$

Assuming that the boundary Γ can be approximated by a polygon consisting of k segments, the displacement $\mathbf{u}$ due to a uniformly distributed load $\mathbf{p}$, acting on the region Ω of the non-homogeneous half-space is, analogous to (2), given by

$$\mathbf{u} = \mathbf{\Theta p} \tag{21}$$

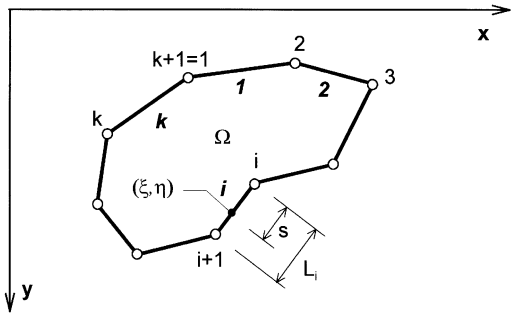

Figure 4. Polygonal approximation of the loaded area Ω

where $\mathbf{u} = (u_x, u_y, u_z)^T$, $\mathbf{p} = (p_x, p_y, p_z)^T$ and $\boldsymbol{\Theta}$ is defined by

$$\boldsymbol{\Theta} = \frac{1}{m_E}\begin{bmatrix} \vartheta_{xx} & \vartheta_{xy} & \vartheta_{xz} \\ \vartheta_{yx} & \vartheta_{yy} & \vartheta_{yz} \\ \vartheta_{zx} & \vartheta_{zy} & \vartheta_{zz} \end{bmatrix} \tag{22}$$

A typical matrix element ϑ_{rs}, r and s referring to the co-ordinate directions x, y, z is given by

$$\vartheta_{rs}(x, y) = \sum_{i=1}^{k} \int_{L_i} \frac{\partial \Phi_{rs}}{\partial n}\, \mathrm{d}s \tag{23}$$

Segment i joins the points on the boundary with co-ordinates (ξ_i, η_i) and (ξ_{i+1}, η_{i+1}) and segment k joins the point (ξ_k, η_k) and $(\xi_{k+1}, \eta_{k+1}) = (\xi_1, \eta_1)$ as shown in Figure 4. The sum runs over all k segments by which the boundary Γ of the loaded area Ω is discretized, and the integrand in (23) is given by (20).

Using the notation depicted in Figure 4, the length of segment i takes the form

$$L_i = \sqrt{(\xi_{i+1} - \xi_i)^2 + (\eta_{i+1} - \eta_i)^2} \tag{24}$$

and for a point (ξ, η) lying on segment i we have

$$\begin{aligned} \xi &= \xi_i + \frac{s}{L_i}(\xi_{i+1} - \xi_i) \\ \eta &= \eta_i + \frac{s}{L_i}(\eta_{i+1} - \eta_i) \end{aligned} \tag{25}$$

According to Gauss's theorem, the normal on the boundary Γ is outwardly directed. Hence the normal vector $\mathbf{n}_i$ on a segment i which is defined by the direction cosines $n_{i\xi}$ and $n_{i\eta}$, is given by

$$\begin{aligned} n_{i\xi} &= +\frac{\eta_{i+1} - \eta_i}{L_i} \\ n_{i\eta} &= -\frac{\xi_{i+1} - \xi_i}{L_i} \end{aligned} \tag{26}$$

With these definitions the integral in (23) can be evaluated numerically in a standard manner by applying Gauss–Legendre quadrature. It should be noted that we have now transformed our problem, which formerly required the solution of a two-dimensional integral, into a series of one-dimensional integrals corresponding to the discretization of the boundary of the loaded area as indicated by (23). Using this approach, difficulties in the numerical integration associated with the singularity, particularly when α tends towards unity, are overcome.

4. NUMERICAL RESULTS

In order to check the method proposed some numerical results are presented in this section. First of all a homogeneous half-space subjected to uniform tractions acting on a rectangular area was considered. The comparison of the results based on this method showed perfect agreement with analytic solutions published by Giroud[9] for all components of the surface displacements due to vertical and horizontal loading. Since in the current approach both homogeneous and non-homogeneous soils are dealt with in the same manner, the results obtained from the homogeneous half-space provided some evidence for the validity of the present numerical scheme. For a more rigorous check, i.e. when the soil mass is non-homogeneous, the results are compared with solutions given by Booker *et al.*[15] and Booker[19] for the cases of the uniformly, vertically loaded circle and rectangle.

4.1. Uniform vertical loading on a rectangular area—convergence study

In the present approach the boundary of the loaded area on the surface is approximated by a polygon and the solution is found by numerical integration. Therefore, it is obvious that the discretization order and the applied quadrature rule will have some impact on the accuracy of the results. In order to quantify this issue, a uniformly, vertically loaded square on a non-homogeneous half-space is considered in which case the vertical displacements can be compared with the analytic solution given by Booker.[19] To get a more comprehensive view of the solution, rather than looking at deflection values at a certain point, the differences between numerical and analytical results are computed along the section *S–S* of length *L* stretching across the edge of the loaded square in equal parts as depicted in Figure 5.

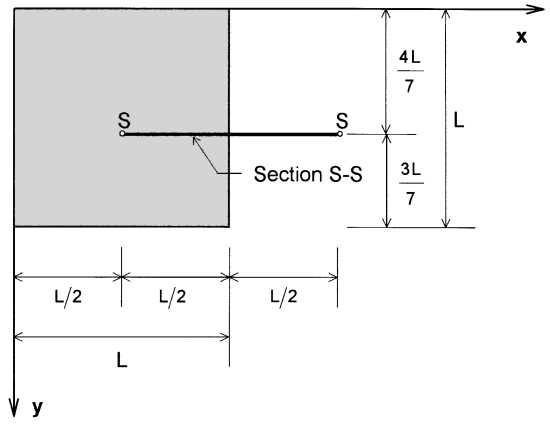

Figure 5. Problem layout

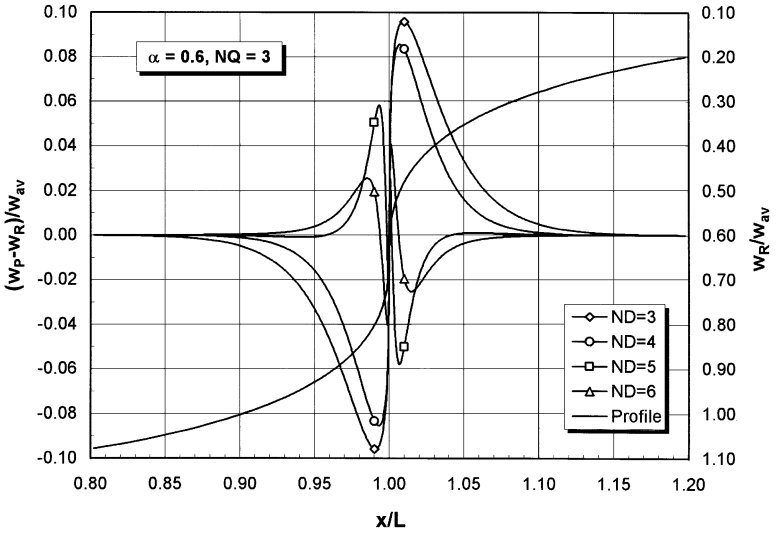

Figure 6. Difference between numerical and analytical solution at the edge of the loading in section *S–S* for quadrature rule $NQ = 3$ and various discretization orders. Non-homogeneous half-space $\alpha = 0{\cdot}6$

The surface deflection along the section was computed using different discretization orders ND and quadrature rules NQ, where a specific value ND refers to the number of segments used for the discretization of one side of the square. The location of the section *S–S* was chosen in a way to enable the calculation of the deflection at the edge of the loaded area for any value of NQ considered in this study, since for cases when the segment lies symmetrical to section *S–S* numerical problems would otherwise arise when NQ takes any odd value. Of course, in a practical application of the numerical procedure, this problem is easily overcome by increasing the quadrature rule to an even value for the segment in question.

Figure 6 shows the normalized differences between analytical and numerical solutions $(w_P - w_R)/w_{av}$, and the deflection profile, w_R/w_{av}, in the vicinity of the edge of the loading along section *S–S*. The notations w_R and w_P refer, respectively, to the settlement calculations based on the analytic solution for the rectangle and the proposed method approximating the boundary of the loading by a polygon. The average settlement underneath the square, w_{av}, was calculated by means of numerical integration using the analytic solution for the rectangle. For all error curves $ND = 3$ to 6 a non-homogeneity parameter $\alpha = 0{\cdot}6$ was assumed and a three-point Gauss quadrature rule was used. From this chart it can be seen that virtually no error is involved if we calculate settlements at locations lying outside the region $0{\cdot}85L \leqslant x \leqslant 1{\cdot}15L$. Within this region the error is distributed antimetrically with respect to the edge of the loaded square and it decreases with increasing discretization order. The maximum normalized error within this region lies between about 10 and 3 percent, and at $0{\cdot}05L$ from the edge between about 3·5 percent for $ND = 3$ and about 0·5 percent for $ND = 6$, as shown in Figure 6.

A detailed study by Stark and Booker[18] shows that the region where a considerable error is involved shrinks with increasing discretization order and quadrature rule. Whereas generally the error is monotonically decreasing for higher values of ND and NQ, this does not seem to be the case near the edge of the loading, where the peak of the error may increase in certain instances. Beyond that, as might be expected, the higher the degree of non-homogeneity, the more concentrated the error becomes at the edge of the loading. It might be noteworthy to point out

that at the very edge of the loading, virtually no difference between numerical and analytical solution can be detected, as shown in Figure 6.

With respect to applying this method in a soil–structure interaction analysis the above example shows that high accuracy can be achieved at reasonable cost. To get the flexibility coefficients, say, in most cases we are calculating the settlements most likely either in the centre or at the edge of the loaded area or at a distance greater than $L/2$ from the edge of the loading. Assuming the use of a discretization order $ND = 3$ and a quadrature rule $NQ = 2$, the error between analytical and numerical solutions for the settlement in the centre of the square for instance would be about 0·005 and 0·003 percent of the average settlement for a non-homogeneity factor $\alpha = 0{\cdot}6$ and $\alpha = 0$.

4.2. Uniform vertical loading on a circular area

In this section the outlined numerical approach will be used to study the deformation behaviour of the non-homogeneous half-space subjected to uniformly distributed loads acting on areas of different shapes. To check the proposed procedure, a circle of a given area is approximated by regular polygons of equivalent area. Increasing the order of the polygon to approximate the circle, the convergence can be assessed and in the limiting case the settlements obtained by using this method should be almost identical to the closed-form solution existing for the uniformly loaded circle (Booker *et al.*[15]). The results of this study may be used as a guideline for the discretization of loaded areas with curved boundaries on both the homogeneous and non-homogeneous half-space.

Six cases are considered where the circle is approximated by regular polygons: triangle, square, hexagon, octagon, decagon and dodecagon, each of the same area as the given circle. All these cases are studied under different non-homogeneity degrees of the soil mass, i.e. the parameter α is varied from zero (homogeneous half-space) to one (Gibson-soil) in steps of 0·2. Because of symmetry the computation may be restricted to a sector with a centre angle φ_c ranging between 60° in the case of the triangle and 15° for the regular 12-sided polygon. As depicted in Figure 7 in the case of a square, this sector is bounded by the sections denoted as 'corner' and 'middle' passing, respectively, from the centre through the corner and from the centre through the middle of the side of the individual polygon.

Figures 8 and 9 show the settlement profiles due to different polygonal approximations, PN, of the circular loading on a non-homogeneous half-space, $\alpha = 0{\cdot}6$, along the respective sections

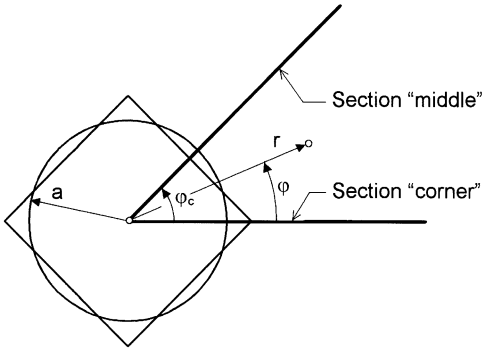

Figure 7. Approximation of a circle by a regular polygon

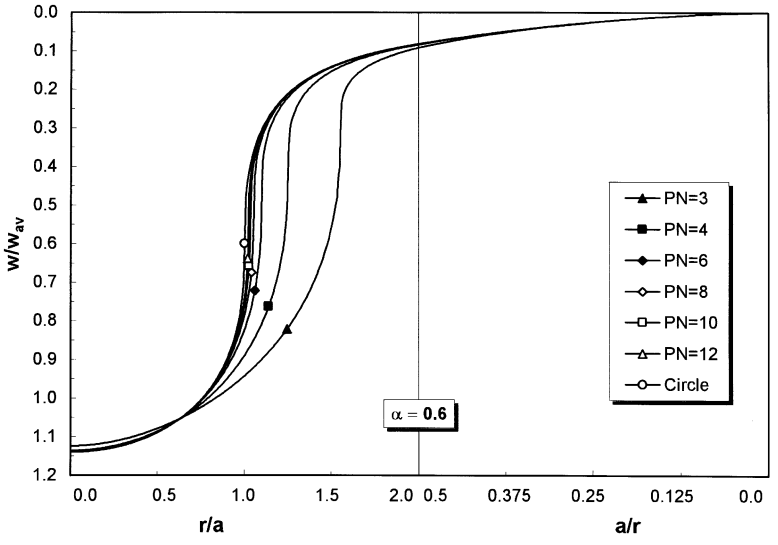

Figure 8. Deflection profiles along the section 'corner'

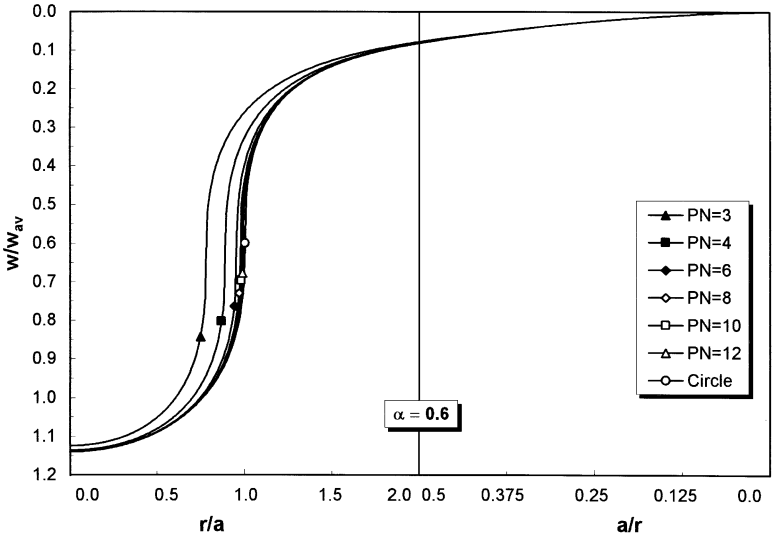

Figure 9. Deflection profiles along the section 'middle'

'corner' and 'middle'. As would be expected, increasing the order of the polygon the settlements tend to the deflection profile obtained from the analytical solution for the circle. These charts are normalized using the average deflection w_{av} underneath the loaded circle given by

$$w_{\mathrm{av}} = \frac{2}{1-\alpha}\frac{P_z B}{m_E a^{(1+\alpha)}}\frac{\Gamma(2-\alpha)}{\Gamma\left(\dfrac{3-\alpha}{2}\right)\Gamma\left(\dfrac{5-\alpha}{2}\right)} \tag{27}$$

where P_z denotes the total vertical load.

To show the full range of the settlement profile in a rational manner without loss of accuracy within and near the loaded area, the distance from the centre is scaled using two different factors. For easier distinction of the two regions, a vertical line is drawn which bisects the charts.

It might be worthwhile to point out that the charts in Figures 8 and 9 all deal with a non-homogeneity parameter $\alpha = 0{\cdot}6$. Although for different values of α the tendency within a specific chart will be the same, the absolute magnitude of the settlement differences with respect to the circular loading vary with α and very much depend on the location under consideration. The bigger α gets, the greater the deflection gradient at the edge of the loading becomes, and therefore the differences at and in the vicinity of the non-matching loaded regions become increasingly larger. On the other hand, away from the edge of the loading, higher values of α lead to smaller settlement differences since the higher α gets, the more uniform the settlement profiles become underneath the loading and the more the settlements are confined to the vicinity of the loaded region.

In order to demonstrate the convergence of the results with the growth of PN for the class of non-homogeneity under consideration, the normalized settlement differences with respect to the circular loading are plotted in Figures 10–12 for various α parameters at three different locations, i.e. at the centre of the loading and at a distance $r/a = 2$ from the centre on the section 'middle' and 'corner'. These figures show that increasing the order of the polygon from 3 to 12 to approximate the circular loading results in a decrease of the settlement differences of about three orders of magnitude at these locations except for the case $\alpha = 1$ where the differences are vanishingly small irrespective of the chosen approximation. The higher the non-homogeneity parameter α becomes, the smaller the differences at these locations. To facilitate comparison of these 3 charts the same log scale was used. Since some of the data in Figure 11 have negative values, i.e. in the case of $3 \leqslant PN \leqslant 6$ and $0 \leqslant \alpha \leqslant 0{\cdot}8$, the norm of these values has been plotted.

So far we have looked at settlements and settlement differences at certain points. Full details are given in Reference 18. To be able to make a statement on the overall error associated with the approximation of the circular loading by regular polygons within an area A the average difference

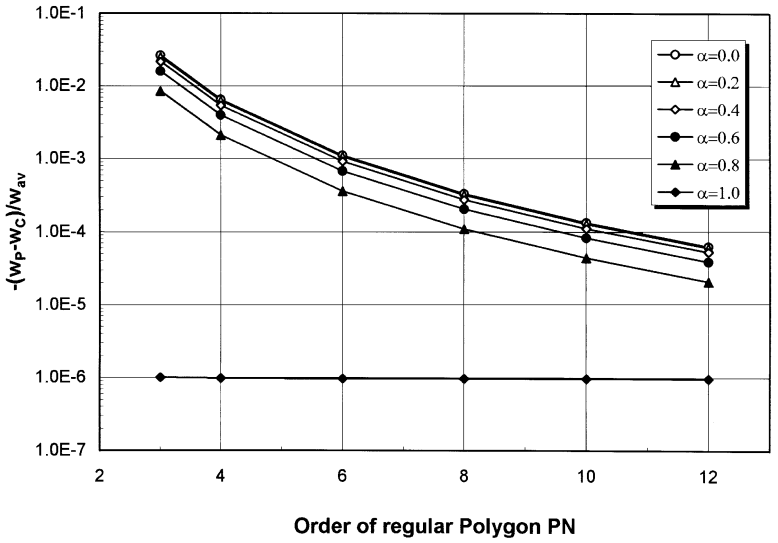

Figure 10. Convergence of the settlement differences at the centre of the loading for different polygonal approximations and various α parameters

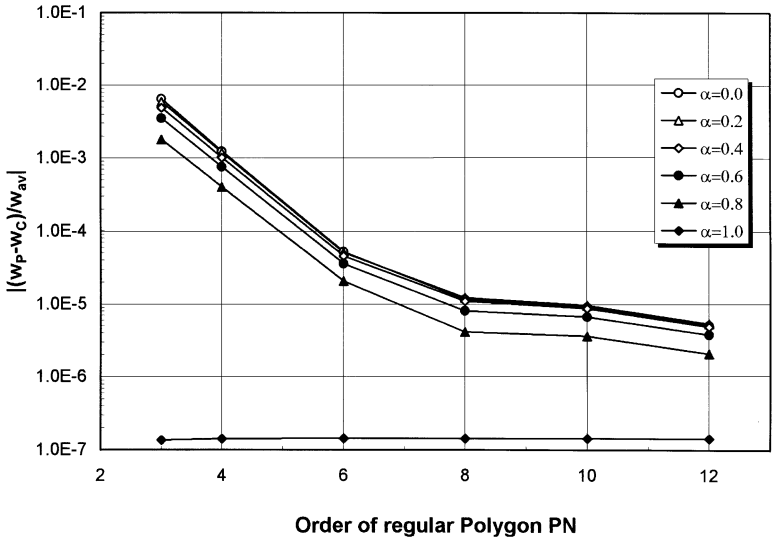

Figure 11. Convergence of the settlement differences at $r/a = 2{\cdot}0$ in the section 'middle' for different polygonal approximations and various α parameters

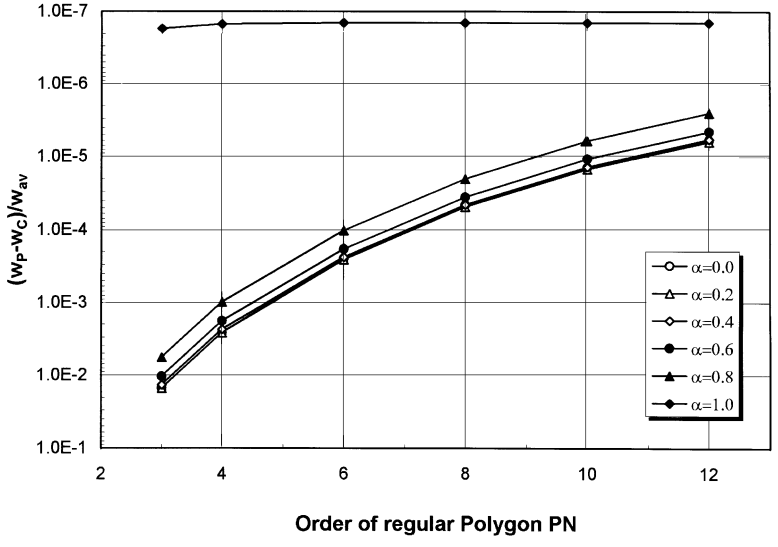

Figure 12. Convergence of the settlement differences at $r/a = 2{\cdot}0$ in the section 'corner' for different polygonal approximations and various α parameters

δ_{av} is considered as an adequate measure and is defined by

$$\delta_{av} = \frac{2}{w_{av} a^2 \varphi_c} \int_A |w_P - w_C| \, dA . \tag{28}$$

a denotes the radius of the loaded circle and φ_c the centre angle bounding the computation sector as shown in Figure 7. Using the above normalization both the size of the loading and the effect of

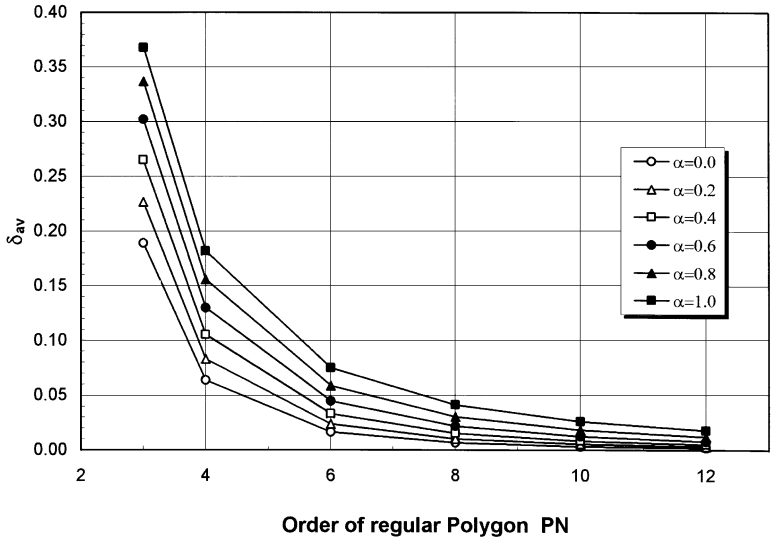

Figure 13. Convergence of the average settlement differences between regular polygon and circle on the entire surface

Poisson's ratio of the soil are eliminated. It should be mentioned that the differences are not added up algebraically, since we do not want settlement differences of different signs to be mutually compensated. In the numerical integration scheme the trapezoidal rule was adopted and to account for the infinite integration domain the upper integration limit for r was assumed to be $100a$. Figure 13 allows an assessment of the convergence with increase of the polygonal order. As shown in this chart the solution converges very rapidly for all values of non-homogeneity parameters α. Furthermore, it can be seen that the higher the parameter α, the bigger the average difference between settlements due to the circular loading and a particular polygonal approximation becomes. It might be worthwhile to point out that the fact that the integrated differences are higher for higher values of α, does not necessarily mean that the more homogeneous the base, the less influence the discretization of a curved boundary has, since the error involved in the settlement also depends on the location under consideration, as mentioned earlier.

If an incompressible Gibson soil is considered, the accuracy of the numerical scheme may easily be checked. In this case the integrated differences δ_{av} between the settlements due to the uniformly loaded circle and a polygon of equivalent area as given by equation (28) should tend to the analytic expression defined by

$$\delta_{\mathrm{av,analytic}} = \frac{2}{a^2 \varphi_c} \sum \Delta A_{\mathrm{CP}} \tag{29}$$

where $\sum \Delta A_{\mathrm{CP}}$ denotes the sum of all non-matching areas of the circle and polygon. It should be noted that close agreement between numerical and analytical results is only obtained if the spacing of the points in radial direction where displacements are calculated is small enough to capture the jump of the displacements at the transition form the loaded to the unloaded region. To facilitate an assessment of the results for this case equation (29) has been evaluated. As might be seen from Figure 13 and Table I the numerical results are in satisfactory agreement with the corresponding analytic values for all orders of regular polygons PN.

Table I. Analytic results for the average settlement differences between regular polygon and circle on the entire surface for an incompressible Gibson soil

PN	3	4	6	8	10	12
Equation (29)	0·3649	0·1810	0·0745	0·0408	0·0258	0·0178

5. CONCLUSIONS

A numerical scheme has been developed which may be used to calculate the surface displacements of both the homogeneous and non-homogeneous half-space, subject to uniformly distributed tractions acting on an arbitrarily shaped area of the surface. The non-homogeneity is related to Young's modulus E which is assumed to vary with depth z in the form $E = m_E z^{\alpha}$ where m_E is a constant and the non-homogeneity parameter α takes values between zero and unity. Poisson's ratio is assumed to be constant. The arbitrarily shaped area where the load is applied is linearized piecemeal and the integration is carried out over the boundary of the loaded domain. By appropriate transformation the double integral is broken up into a series of one-dimensional integrals and the inherent singularity which becomes more pronounced the greater the degree of the non-homogeneity, no longer constitutes any problem. Comparison with existing analytic solutions for the surface settlement of the non-homogeneous half-space due to uniform vertical loading shows excellent agreement for both the rectangular and circular shaped areas. In an example the possible error in the settlements stemming from the discretization of a curved boundary of the loaded area was assessed. It was shown that the discretization order of such a boundary should be chosen with regard to the location of the settlement to be evaluated and the degree of non-homogeneity. The higher the non-homogeneity the less influence the discretization of the boundary has on settlements at locations away from the edge of the loading. But, on the other hand, at the same time the discretization might be crucial if settlements are to be computed at the edge or near the edge of the loaded domain. With respect to application in a soil–structure interaction analysis the method proposed enables the calculation, say, of the flexibility coefficients for arbitrarily shaped elements emanating from the discretization process of the foundation structure.

APPENDIX

According to Booker *et al.*[14] the coefficients A, B, H, K, L are given by the following equations;

$$
\begin{aligned}
A &= \frac{a}{\Theta_{\alpha}} = -L \\
B &= \frac{b}{\Theta_{\alpha-1}} \\
H &= \frac{h+k}{2\Theta_{\alpha-1}} + \frac{h-k}{2(2\Theta_{\alpha+1} - \Theta_{\alpha-1})} \\
K &= \frac{h+k}{2\Theta_{\alpha-1}} - \frac{h-k}{2(2\Theta_{\alpha+1} - \Theta_{\alpha-1})}
\end{aligned}
\tag{30}
$$

where a, b, h, k, l are found to be

$$\begin{aligned} a &= \frac{1-\nu^2}{\alpha}\cos\frac{\beta\pi}{2}F_{\alpha\beta} = -l \\ b &= \frac{1-\nu^2}{\alpha}\sin\frac{\beta\pi}{2}F_{\alpha\beta}\frac{\beta}{\alpha+1} \\ h &= \frac{1-\nu^2}{\alpha}\sin\frac{\beta\pi}{2}F_{\alpha\beta}\frac{\alpha+1}{\beta} \\ k &= \frac{2(1+\nu)}{\alpha\Theta_\alpha} \end{aligned} \tag{31}$$

$\Theta_{(a+m)}$ is defined by

$$\Theta_{(\alpha+m)} = \frac{\Gamma\left(\frac{(\alpha+m)+1}{2}\right)\Gamma\left(\frac{1}{2}\right)}{\Gamma\left(\frac{(\alpha+m)+2}{2}\right)} \tag{32}$$

where m takes the values $-1, 0, +1$ as shown in equations (30) and (31). Finally, $F_{\alpha\beta}$ and β are given by

$$\begin{aligned} F_{\alpha\beta} &= \frac{2^{(\alpha+1)}}{\pi}(\alpha+2)\frac{\Gamma\left(\frac{3+\alpha+\beta}{2}\right)\Gamma\left(\frac{3+\alpha-\beta}{2}\right)}{\Gamma(3+\alpha)} \\ \beta &= \sqrt{(1+\alpha)\left(1-\frac{\alpha\nu}{1-\nu}\right)} \end{aligned} \tag{33}$$

and Γ denotes the gamma function. It might be noteworthy to point out that for the two limiting cases, i.e. the homogeneous half-space ($\alpha = 0$) we find that $\beta = 1$, $F_{\alpha\beta} = 2/\pi$ and for the incompressible Gibson soil ($\alpha = 1$ and $\nu = 0{\cdot}5$) $\beta = 0$, $F_{\alpha\beta} = 2/\pi$.

Plots of the coefficients $A, B, H + K$, and $H - K$ given in Stark and Booker[18] show that the displacements considerably depend on the degree of non-homogeneity, α, and that the influence of Poisson's ratio increases with increasing α.

ACKNOWLEDGEMENT

The work described in this paper was sponsored by the Austrian Science Foundation, grants no. J0702-Tec and J0963-Tec. This support is gratefully acknowledged.

REFERENCES

1. R. E. Gibson, 'Some results concerning displacements and stresses in a non-homogeneous elastic half-space', *Géotechnique*, **17,** 58–67 (1967).
2. P. T. Brown and R. E. Gibson, 'Surface settlement of a deep elastic stratum whose modulus increases linearly with depth', *Can. Geotech. J.*, **9,** 467–476 (1972).
3. R. E. Gibson, P. T. Brown and K. R. F. Andrews, 'Some results concerning displacements in a non-homogeneous elastic layer', *Zeit. ang. Math. Phys.*, **22,** 855–864 (1971).

4. K. Fischer, *Beispiele zur Bodenmechanik. Aufsätze mit Formeln, Tafeln und Schaubildern*, Wilhelm Ernst & Sohn, Berlin, 1965.
5. R. K. Rowe and J. R. Booker, 'The behaviour of footings resting on a non-homogeneous soil mass with a crust. Part I—Strip footings', *Can. Geotech. J.*, **18,** 250–264 (1981a).
6. R. K. Rowe and J. R. Booker, 'The behaviour of footings resting on a non-homogeneous soil mass with a crust. Part II—Circular footings', *Can. Geotech. J.*, **18,** 265–279 (1981b).
7. L. N. Repnikov 'Calculation of beams on an elastic base combining the deformative properties of a Winkler base and an elastic mass', *Soil Mech. and Found. Eng.* (*USSR*), **4,** 384–389 (1967).
8. E. Schulze, 'Die Kombination von Bettungszahl- und Steifezahlverfahren', VGB Mitteilungen, **48,** Achen, 1970.
9. J. P. Giroud, *Mèchanique des sols. Tables pour la calcul des foundations*, Vols. 1 and 2, Dunod, Paris, 1972 and 1973.
10. F. G. Butler, '*Heavily Overconsolidated Clays*', *COSOS*: *Settlement of Structures*, *Conf.* Cambridge, London, Pentech Press, 1975.
11. O. K. Fröhlich, Druckverteilung im Baugrunde, Springer, Wien, 1934.
12. J. Ohde, 'Zur Theorie der Druckverteilung im Baugrund', *Der Bauingenieur*, **20,** 451–459 (1939).
13. D. L. Holl, 'Stress transmission in earth', *Proc. High. Res. Board*, **20,** 709–721 (1940).
14. J. R. Booker, N. P. Balaam and E. H. Davis, 'The behaviour of an elastic, non-homogeneous half-space. Part I—line load and point loads', *Int. j. numer. anal. Methods Geomech.*, **9,** 353–367 (1985a).
15. J. R. Booker, N. P. Balaam and E. H. Davis, 'The behaviour of an elastic, non-homogeneous half-space. Part II—circular and strip footings', *Int j. numer. anal. methods geomech.*, **9,** 369–381 (1985b).
16. Y. K. Cheung and O. Z. Zienkiewicz, 'Plates and tanks on elastic foundations—An application of finite element method', *Int. j. solids struct.*, **1,** 451–461 (1965).
17. Y. K. Chow, 'Vertical deformation of rigid foundations of arbitrary shape on layered soil media', *Int. j. numer. anal. methods geomech.*, **11,** 1–15 (1987).
18. R. F. Stark and J. R. Booker, 'A numerical procedure for calculating the flexibility matrix of a non-homogeneous elastic half-space subjected to uniform surface tractions. Part I—arbitrarily shaped foundations', *Research Report R697*, University of Sydney, School of Civil and Mining Engineering, 1994.
19. J. R. Booker, 'Analytic methods in geomechanics', in *Proc.* G. Beer, J. R. Booker, J. P. Carter (eds) *7th Int. Conf. Computer Meth. Advances Geomechanics,* Vol. **1,** 1991, pp. 3–14.

